Visibility Constrained Surface Evolution

Jan Erik Solem[1], Fredrik Kahl[2] and Anders Heyden[1]

[1]Applied Mathematics Group, School of Technology and Society, Malmö University, Sweden
[2]Dept. of Computer Science & Engineering, University of California, San Diego, La Jolla CA
jes@ts.mah.se, fredrik@maths.lth.se, heyden@ts.mah.se

Abstract

The problem of feature-based surface reconstruction is considered in this paper. Our main contribution is the ability to handle visibility constraints, obtained from the projections of points, curves and silhouettes, in the surface fitting process. While traditional methods often ignore such information, we show that visibility constraints not only give better initial surface estimates and faster convergence, but also provide an important cue for determining surface topology.

The problem is cast as a variational problem with constraints within the level set framework. It is shown how to evolve the surface without violating the visibility constraints using methods from variational calculus. Applications of the theory are detailed for a number of important cases of geometric primitives: points, curves and visual hulls. Several experiments on real image sequences are given to demonstrate the performance of the approach.

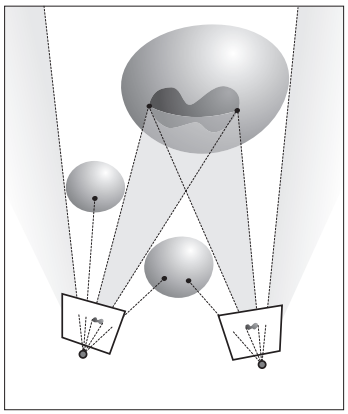

Figure 1: The visual rays between image features and scene features provide constraints on the surface geometry.

1. Introduction

Reconstructing scene models from images is a classical (inverse) problem in computer vision. The most common techniques for obtaining a dense 3D model can be categorized as (i) multi view stereo which gives a camera centered representation in the form of *depth maps* [14], (ii) volumetric approaches such as *space carving* [8] and (iii) *surface fitting* which gives a scene centered representation in the form of surfaces [2, 23, 6]. This paper will pursue the scene centered approach by fitting a surface to (sparsely) reconstructed scene features.

State of the art structure from motion systems usually only reconstruct the scene as a set of points [5], usually referred to as *point clouds*. Fitting a surface to these points has turned out to be a challenging problem since there is no information regarding the connectivity of the points or the topology of the true surface. Also, the density of the points may vary greatly over the scene.

When representing the surface, one has to choose between explicit and implicit surface representations. Recently, there has been a lot of activity using implicit representations, especially in the area concerning level set methods [13]. The variational level set method is a frequently used framework where the surface motion is derived as the gradient descent of a functional, cf. e.g. [22].

The present paper deals with the variational level set method applied to the case of surface fitting to data obtained from the motion, the images and 3D features. In the simplest form, surfaces are fitted to *unorganized* 3D points, i.e. there is no information regarding the connectivity of the points, cf. [23]. Given observations in images where scene points, curves or contours are visible, the surface should evolve so that visual rays between the scenes features and their projections are never crossed, cf. Figure 1. In other words, the surface should never move in a direction such that it occludes the visible parts. As will be shown, this gives a constrained variational problem. The derivations are performed for a general class of functionals and then specialized to the case of surface fitting to unorganized points and visual hulls.

When fitting surfaces to unorganized points, visibility observations give valuable information. By observing points on the surface, points in the background or bound-

ing contours, difficult questions regarding the topology of the surface can be answered. This fits nicely with the use of the level set method as it can represent surfaces that can change topology automatically. The framework introduced can also incorporate other constraints such as e.g. that the surface has to be in front of the cameras (known as chirality [4]) or that the surface is restricted to a predefined volume in space of any shape.

Related Work This work is most closely related to the popular surface fitting method of Zhao et. al. [23] where level sets are fitted to point clouds. It was extended to incorporate image correlation in a robust manner in [9].

Visibility information has previously been applied in a discrete setting for different purposes. In [7] scenes are reconstructed using graph cuts. In [4], chirality is used to improve upon point cloud reconstructions. Chirality has also successfully been applied as an auto-calibration constraint [12]. In [11], an algorithm for producing a triangular mesh for sparse 3D structure is developed which is guaranteed to obey visibility constraints for point and line features. In a similar spirit, by reasoning about *freespace*, a principle for guiding surface triangulation is derived in [21]. The main difference to our work is that we are using a continuous framework both for the surface representation and evolution and for representing the visibility constraints. This leads to the formulation of a variational problem. In this setting, matters concerning for example smoothness or shape priors are naturally handled. Furthermore, by using a level set representation, surface topology can automatically be inferred.

Our framework also applies to visual hull reconstructions. The literature on this topic is vast, e.g. [18, 1, 20]. Again, most of the approaches work in a discrete setting by either voxel carving or triangular meshing. In contrast, our approach provides a continuous framework which simultaneously estimates the visual hull *and* at the same time enforces smoothness constraints. In addition, it is possible to combine visual hull constraints with those of surface fitting to point, curve and silhouette features.

2. Background

As a courtesy to the reader, the necessary background on the level set method and how to derive gradient descent procedures for variational formulations are briefly described here.

2.1. Level Set Representation

The time dependent surface $\Gamma(t)$ is represented implicitly as the zero level set of a function $\phi(\mathbf{x}, t) : \mathbf{R}^3 \times \mathbf{R} \to \mathbf{R}$ as

$$\Gamma(t) = \{\mathbf{x}\,;\ \phi(\mathbf{x}, t) = 0\}\ . \tag{1}$$

The sets $\{\mathbf{x}\,;\ \phi(\mathbf{x}, t) < 0\}$ and $\{\mathbf{x}\,;\ \phi(\mathbf{x}, t) > 0\}$ are called the *interior* and the *exterior* of Γ, respectively. The interior of Γ is denoted Ω^-. Using this definition the outward unit normal $\mathbf{n}$ and the mean curvature κ are given as

$$\mathbf{n} = \frac{\nabla\phi}{|\nabla\phi|} \quad \text{and} \quad \kappa = \nabla \cdot \frac{\nabla\phi}{|\nabla\phi|}\ . \tag{2}$$

One important, frequently used example is the signed distance function, where the additional requirement $|\nabla\phi| = 1$ is imposed.

To evolve the surface according to some derived velocity $\mathbf{v}$, a PDE of the form

$$\frac{\partial\phi}{\partial t} + \mathbf{v} \cdot \nabla\phi = 0 \quad \text{or} \quad \frac{\partial\phi}{\partial t} + v_n|\nabla\phi| = 0\ , \tag{3}$$

is solved, where v_n is the velocity normal to the surface. For a more thorough treatment of the level set method and implicit surface representations, cf. [13].

2.2. Variational Formulations

Let $\Psi : \mathbf{R}^3 \times S^2 \to \mathbf{R}$ be a general function that can depend on surface point $\mathbf{x}$ and surface normal $\mathbf{n}$. Define the general functional as the surface integral

$$f(\Gamma) = \int_\Gamma \Psi(\mathbf{x}, \mathbf{n})\, d\sigma\ , \tag{4}$$

where Γ is the surface and $d\sigma$ the Euclidean surface measure. This general case covers many variational formulations for computer vision problems. Examples of common functionals can be found in e.g. [3, 19].

If Γ is embedded as the zero set of ϕ, the Euler-Lagrange equation for $f(\Gamma)$ is an equation of the form

$$\mathbf{F}\delta(\phi) = 0\ , \tag{5}$$

where $\delta(\phi(\mathbf{x}))$ is the pullback of the Dirac distribution δ by ϕ and it appears as the variation is taken over the surface Γ. It can be shown that for the case (4), the expression for $\mathbf{F}$ is given by[1]

$$\mathbf{F} = \nabla \cdot [\nabla_{S^2}\Psi + \Psi\,\mathbf{n}]\ . \tag{6}$$

Minimizing $f(\Gamma)$ using gradient descent gives an equation of motion as

$$\frac{\partial\phi}{\partial t} = \mathbf{F}|\nabla\phi|\ , \tag{7}$$

where the normal velocity is $v_n = -\mathbf{F}$. For details on deriving the motion equation for general functionals of the form (4) and the formula (6), see [3, 19].

3. Visibility Constrained Evolution

This section describes how to evolve surfaces in a variational level set formulation such that visibility conditions are fulfilled at all times during the evolution. The theory is developed for a general functional of the form (4) and in the next section it will be specialized to treat surface fitting to 3D data.

[1] Here ∇_{S^2} is the gradient on the unit sphere S^2.

3.1. Visibility Constraints

If a 3D point is visible from a certain viewpoint, the surface should not cross the line segment joining the camera center and the point itself, cf. Figure 1. Similarly for curves, given a 3D curve and its projection in an image, the surface should not intersect the visual cone with vertex at the camera center.

Another type of constraint of similar character arises from bounding silhouettes. The surface is confined to lie on one side of the back-projected cone of the apparent contour as seen from the viewpoints. This is the basis for all reconstruction methods based on visual hulls, see for example [1]. However, they generally start with carving off forbidden voxels and then proceed by applying some surface fitting technique. Here, it will be an integrated part of the surface fitting procedure.

Similar arguments can be made to find whole volumes that should be free space such as, for example, the region behind the cameras or by intelligent reasoning about structure [21]. Denote the union of all these line segments, visual cones and volumes as the set $W \subset \mathbf{R}^3$. Represent this set as

$$W = \{\mathbf{x}\,;\; w(\mathbf{x}) \geq 0\} \ , \tag{8}$$

using a signed distance function $w : \mathbf{R}^3 \rightarrow \mathbf{R}$. This means that the boundary of this set is the surface[2] $\partial W = \{w = 0\}$, i.e. the zero level set of w.

We will now introduce a measure, in the form of a non-negative functional, to detect if the visibility condition is violated. Define the functional as

$$g(\Gamma, W) = \int_{\Omega^- \cap W} d\mathbf{x} = \int_{\mathbf{R}^3} H(w)(1 - H(\phi))\, d\mathbf{x} \ , \tag{9}$$

where $H(\cdot)$ is the Heaviside function. This functional measures the volume of the intersection of the surface interior and the forbidden subset, $\Omega^- \cap W$. If $g(\Gamma, W) > 0$ this indicates that the surface occludes visible parts of the scene. The visibility constraint is then that $g = 0$. The Euler-Lagrange equation for (9) is simply

$$-H(w)\delta(\phi) = 0 \ . \tag{10}$$

This fact will be used for the surface evolution.

3.2. Constrained Evolution

The surface evolution problem of evolving Γ such that no seen parts (points, curves, background etc) are occluded leads to a variational problem of minimizing f under the constraint $g = 0$. This is solved using Rosen's gradient projection method [15]. Taking a descent PDE for the functional

$$E(\Gamma, W) = f(\Gamma) + \lambda\, g(\Gamma, W) \ , \tag{11}$$

gives the motion equation for the embedded surface as

$$\frac{\partial \phi}{\partial t} = (\mathbf{F} - \lambda H(w))|\nabla \phi| \ . \tag{12}$$

The Lagrange multiplier λ is updated as the surface evolves and is given by the expression

$$\lambda = \frac{\int_{\mathbf{R}^3} \mathbf{F} H(w)|\nabla\phi|\delta(\phi)\, d\mathbf{x}}{\int_{\mathbf{R}^3} (H(w))^2 |\nabla\phi|\delta(\phi)\, d\mathbf{x}} = \frac{\int_\Gamma \mathbf{F} H(w)\, d\sigma}{\int_\Gamma (H(w))^2\, d\sigma} \ , \tag{13}$$

since if the visibility constraint holds at all times then the following relation

$$\begin{aligned} 0 \;&=\; \frac{d}{dt} g(\Gamma, W) = \int_{\mathbf{R}^3} H(w) \frac{d}{dt}\left(1 - H(\phi)\right)\, d\mathbf{x} = \\ &=\; -\int_{\mathbf{R}^3} H(w)\delta(\phi)\frac{\partial \phi}{\partial t}\, d\mathbf{x} = \\ &=\; -\int_{\mathbf{R}^3} H(w)\mathbf{F}\delta(\phi)|\nabla\phi|\, d\mathbf{x} + \\ &\quad +\lambda \int_{\mathbf{R}^3} (H(w))^2 \delta(\phi)|\nabla\phi|\, d\mathbf{x} \ , \end{aligned} \tag{14}$$

must be satisfied.

This means that solving the evolution equation (12) with λ from (13) moves the surface to decrease the energy f and, given that the initial surface satisfies $g = 0$, the visibility criteria are never violated.

It is simple to make the initial surface satisfy the visibility criteria. Since $\Omega^- \setminus W = \Omega^- \cap W^c = \{\mathbf{x}\,;\; \max(\phi(\mathbf{x}), w(\mathbf{x})) \leq 0\}$, any initial value $\phi(\mathbf{x}, 0)$ can be changed such that $g = 0$ by setting

$$\phi(\mathbf{x}) = \max(\phi(\mathbf{x}), w(\mathbf{x})) \ . \tag{15}$$

One inferior alternative to the constrained variational formulation above is to evolve the surface without constraints using (7) and project the result outside the forbidden region at each iteration using (15). The problem with this approach is that it can give an evolution where (7) move Γ repeatedly into the forbidden region W and gets projected outside again. Such oscillatory behavior is undesirable and inferior to using (12) and (13).

Finally, the set of signed distance functions representing surfaces that satisfy the visibility criteria can be shown to be a convex set. Let V denote the set of functions $h : \mathbf{R}^3 \rightarrow \mathbf{R}$, representing surfaces according to the convention in Section 2.1, such that their zero set satisfies the visibility criteria

$$\int_{\mathbf{R}^3} H(h(\mathbf{x}))(1 - H(\phi(\mathbf{x})))\, d\mathbf{x} = 0 \ .$$

[2] In fact this is a manifold of dimension 1 or 2 since the line segments are 1D objects. As will be seen in Section 5, ∂W can be treated as a surface.

This can also be written $V = \{h\ ;\ h \geq -w\}$ if h and w are signed distance functions. It is clear that V is a convex set, i.e. $th_1 + (1-t)h_2 \in V$ for any two functions $h_1, h_2 \in V$ and $t \in [0,1]$, since

$$th_1 + (1-t)h_2 \geq t(-w) + (1-t)(-w) = -w \ .$$

This fact is useful for proving that problems are well-posed.

4. Surface Fitting to 3D Data

This section shows how to evolve surfaces for fitting them to 3D data containing points and curves. Let the 3D data be denoted by the set $\mathcal{S}$. The functional to be minimized is

$$f(\Gamma) = \int_\Gamma d(\mathbf{x})\, d\sigma \ , \tag{16}$$

where $d(\mathbf{x}) = \mathrm{dist}(\mathbf{x}, \mathcal{S})$ is the distance from the point $\mathbf{x}$ to $\mathcal{S}$ as in [23]. The Euler-Lagrange equation for (16) gives

$$\mathbf{F} = (\nabla d \cdot \mathbf{n} + d\kappa) \ . \tag{17}$$

Hence, the constrained version of the complete evolution PDE is found to be

$$\frac{\partial \phi}{\partial t} = (\nabla d \cdot \mathbf{n} + d\kappa - \lambda H(w))\,|\nabla \phi| \tag{18}$$

$$\lambda = \frac{\int_\Gamma (\nabla d \cdot \mathbf{n} + d\kappa) H(w)\, d\sigma}{\int_\Gamma (H(w))^2\, d\sigma} \tag{19}$$

by combining (12) and (13). The details on the standard procedure of surface fitting using (16) can be found in [23].

5. Numerical Implementation

The motion PDE is solved on a fixed equidistant grid in the volume of interest. At all times during the evolution the functions ϕ and w are kept to be signed distance functions.

In Sections 3 and 4 the Heaviside function and Dirac distribution H and δ occur frequently. In practice it is necessary to introduce continuous approximations. Here H is a C^2 approximation and δ a C^1 approximation defined as in [22] as

$$H(x) = \begin{cases} 1 & x > \epsilon \\ 0 & x < -\epsilon \\ \frac{1}{2}[1 + \frac{x}{\epsilon} + \frac{1}{\pi}\sin(\frac{\pi x}{\epsilon})] & |x| \leq \epsilon \ , \end{cases}$$

and

$$\delta(x) = \frac{d}{dx}H(x) = \begin{cases} 0 & |x| > \epsilon \\ \frac{1}{2\epsilon}[1 + \cos(\frac{\pi x}{\epsilon})] & |x| \leq \epsilon \ . \end{cases}$$

The line-of-sight constraint arising from the fact that a 3D point is visible from a viewpoint give a forbidden region as a line. To be able to measure this constraint on a fixed grid it is represented as a tube with radius $\varepsilon > 0$ as $w(\mathbf{x}) = \varepsilon - d_l(\mathbf{x})$, where $d_l(\mathbf{x})$ is the distance to the line. Typically, ε is set to some fraction of a grid cell, i.e. $0 < \varepsilon < 1$.

Once all constraints are determined and represented with functions w_i as the sets $\{\mathbf{x}\ ;\ w_i(\mathbf{x}) \geq 0\}$ for $i = 1, \ldots, N$, the function w in (8) is simply

$$w(\mathbf{x}) = \max(w_1(\mathbf{x}), \ldots, w_N(\mathbf{x})) \ .$$

Finally, the boundary of the region is cleaned up with continuous morphological operations (opening/closing) to remove small protrusions and holes in the set W using a version of the operations defined in [16].

6. Experiments

In this section the proposed method is tested on synthetic and real data for several different cases of visibility constraints. For some examples the surface is visualized using triangulation with the marching cubes algorithm [10] and for all examples the equations (18) and (19) are used. The experiments are chosen to illustrate the benefits of using visibility constraints. Note that there are many different choices for functionals that can be used for these surface reconstruction problems. *Our intent is only to show the positive effects of adding visibility constraints, not to evaluate or compare surface reconstruction methods.*

Synthetic test data with points on a torus was created together with a visibility criteria corresponding to a clear line of sight along the symmetry axis of the torus. The initial surface was a sphere enclosing the torus, projected using $\max(\phi, w)$ to give the surface shown in Figure 2a. The evolution is shown in Figure 2. It can be seen that the proposed method with evolution according to (18) gives the desired motion while using standard evolution and projecting the surface outside the forbidden region at each iteration gives an oscillatory motion where the surface repeatedly moves into the forbidden region and gets projected outside again.

Figure 3 shows a setup with time-of-flight data obtained using a laser radar system. Part of the recovered structure, the tree in the foreground, was used as data points for the surface fitting. In this case points are only recovered on the side of the tree facing the scanner. This means that it is necessary to use the techniques for initializing and fitting open surfaces introduced in [17] if one is to use a level set representation. The resulting surface reconstruction is shown in Figure 4 with and without visibility constraints. From the same data set a point cloud is extracted at the depth corresponding to the inside of the room. Figure 5 shows the point set and the resulting surface with and without using visibility constraints. As can be seen the surface fit is better with the constrained motion. The grid size was $40 \times 40 \times 80$ for both the tree and man data.

To illustrate the procedure for bounding silhouettes, i.e. the surface is constrained to stay inside the objects visual

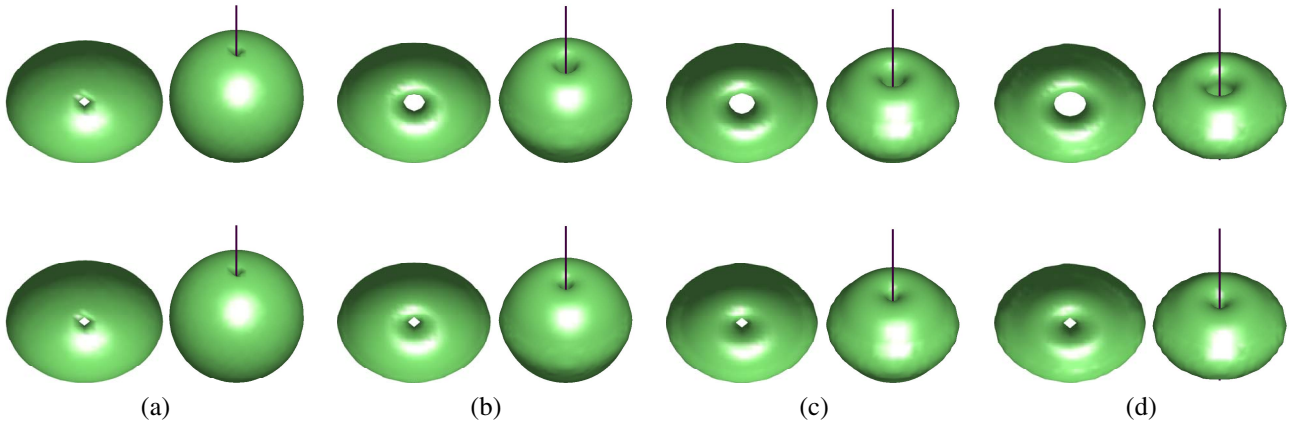

Figure 2: Evolution for surface fitting to points on a torus. (top) proposed evolution with constraints, (bottom) standard evolution with projection to $\max(\phi, w)$ at each iteration. (a) initial surface, (b) after 33 iterations, (c) after 66 iterations, (d) after 100 iterations.

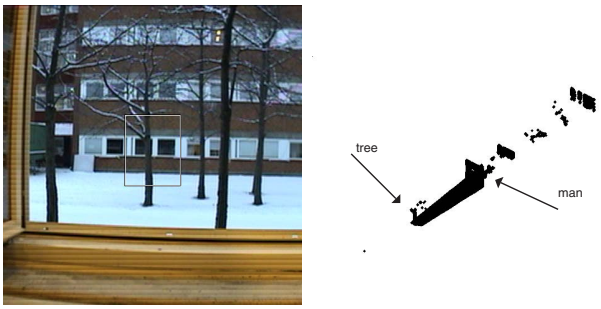

Figure 3: Setup for time-of-flight data where part of the scene is scanned using a short laser pulse. (a) image of the scene with rectangle in the center roughly indicating what is scanned (the actual scanned area does not coincide perfectly with the rectangle), (b) recovered 3D points.

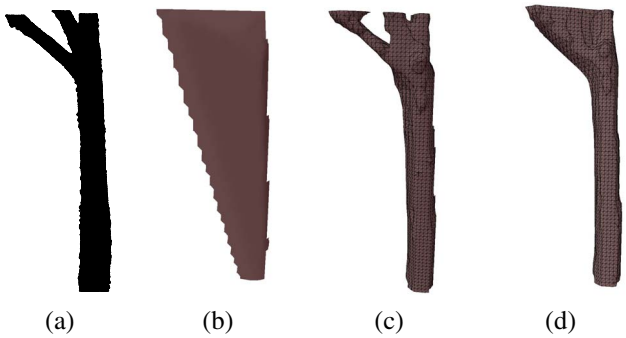

Figure 4: Tree data. (a) recovered 3D points. (b) initial surface. (c) reconstructed surface using visibility constraints and (d) without visibility constraints.

hull, experiments were performed on the Oxford dinosaur data set[3]. The top row of Figure 6 shows three of the 36 images used, together with the recovered 3D structure. The surface of the intersection of the back-projected cones of the silhouettes is shown in the middle row and the bottom row shows the final reconstruction. This gives a continuous silhouette carving formulation since the visual hull is represented as the zero level set of the signed distance function w. The grid size was $100 \times 100 \times 100$.

Finally, we show results for an image sequence of a pitcher[4]. The top row of Figure 7 shows three of the 80 images used, together with the recovered 3D structure. To show the influence of different visibility constraints a surface was fitted to the 3D data without constraints, with line-of-sight constraints from points on the pitcher visible in images and with bounding silhouettes. The results are shown in Figure 7 and a quantitative comparison is shown in Table 1. As can be seen, the correct topology is only recovered with visibility constraints.

7. Conclusions

In this paper we showed how to evolve surfaces in a variational setting such that visibility constraints were never violated. In Section 3 the constraint was formulated using a functional and the constrained surface evolution was derived for a general case. Then we used the concrete example of surface fitting to 3D data to illustrate the procedure in experiments.

The benefits of using visibility; better initial estimates, more consistent surface topology and a better surface fit are

[3] Available at http://www.robots.ox.ac.uk.

[4] Sequence is available at http://homeweb.mah.se/∼tsjeso/downloads/.

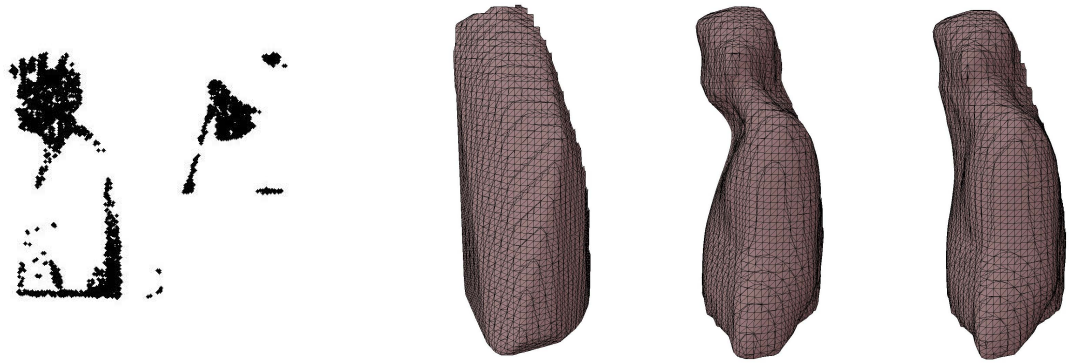

(a) (b) (c) (d)

Figure 5: Man data. (a) part of the recovered 3D points. (b) initial surface. (c) reconstructed surface using visibility constraints in the form of visible background points. (d) reconstructed surface without visibility constraints.

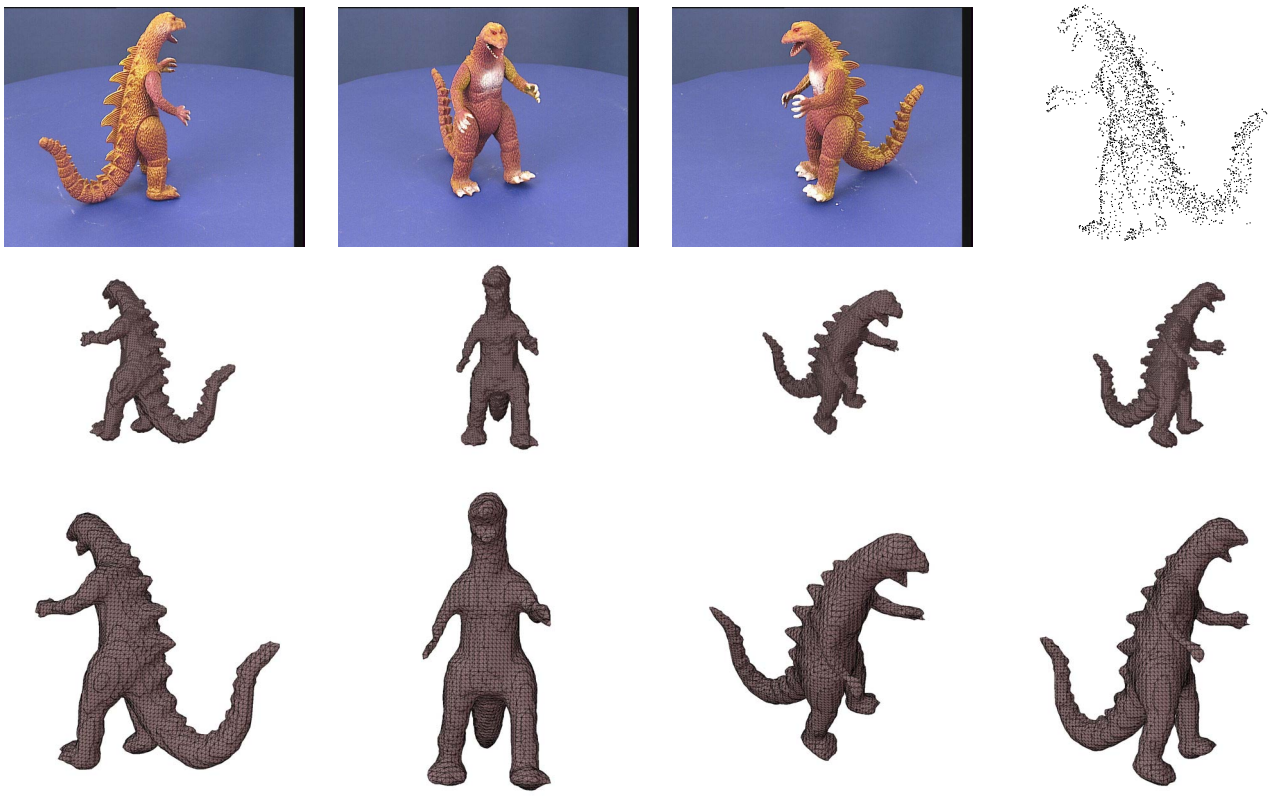

Figure 6: Reconstruction from the Oxford dinosaur sequence. (top) Sample images, frames 1, 10 and 19 out of 36 and recovered 3D points using structure and motion techniques. (middle) the zero surface (triangulated) of the function representing the forbidden region W obtained from bounding silhouettes. (bottom) four views of the reconstructed surface (triangulated), using the constraint that the surface should be inside the surface above.

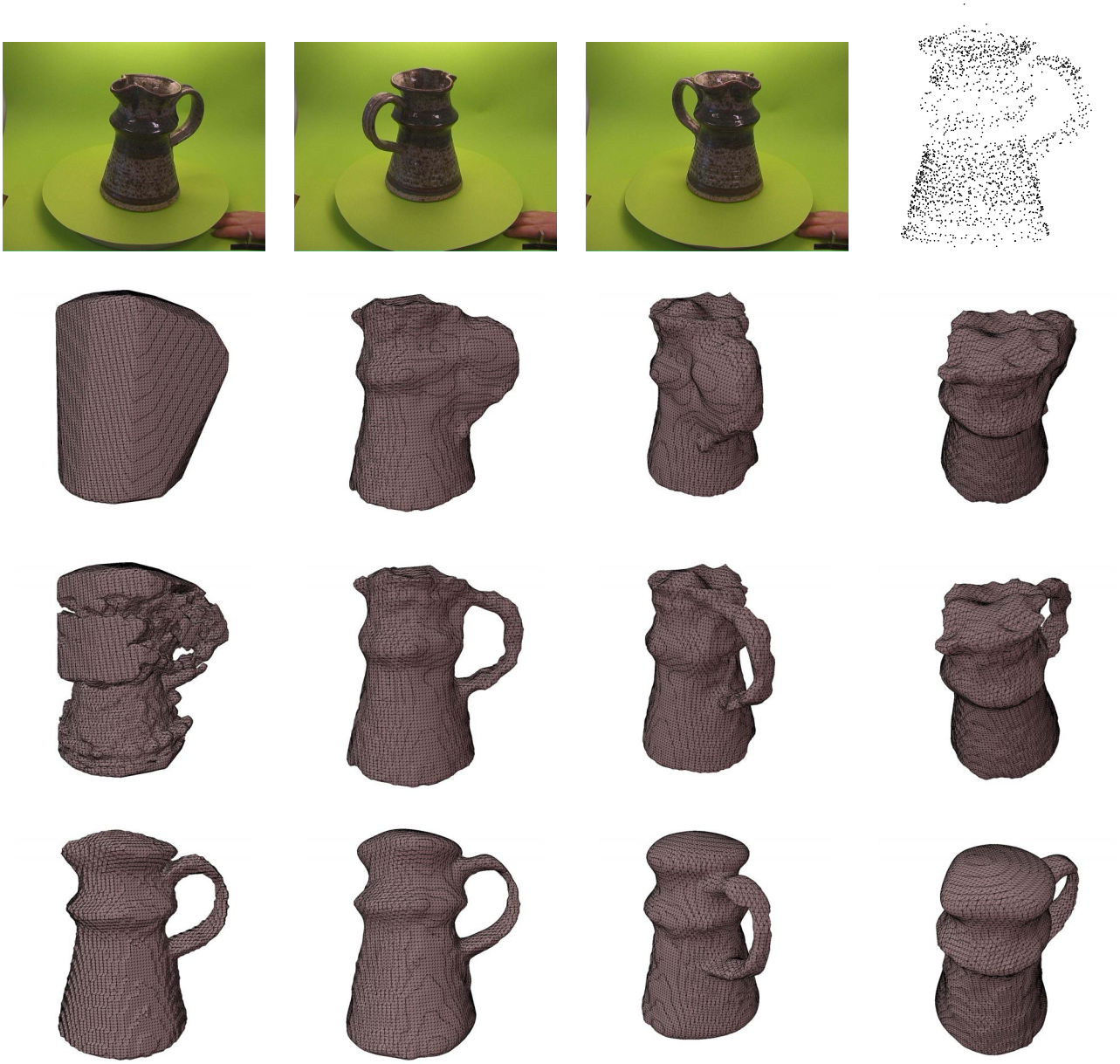

Figure 7: Reconstruction from the pitcher sequence. (top row) Sample images, frames 1, 38 and 56 out of 80 and the 2069 recovered 3D points. (second row) initial surface and 3 views of the final reconstruction without visibility constraints. (third row) initial surface obtained as $\max(\phi, w)$ where w represents a set of line segments computed from points on the pitcher that are visible in images and 3 views of the final reconstruction. (last row) initial surface obtained as $\max(\phi, w)$ where w represents the intersection of bounding silhouettes and 3 views of the final reconstruction.

Constraint	Mean	Median	Grid size	Iterations	Correct topology
none	7.38	6.47	$100 \times 100 \times 100$	268	No
line-of-sight only	7.57	6.44	$100 \times 100 \times 100$	267	Yes
bounding silhouettes only	7.18	6.07	$100 \times 100 \times 100$	21	Yes

Table 1: Comparison for pitcher sequence for different constraints; no constraints, line-of-sight constraints for visible points on pitcher and bounding silhouettes. Mean and median distance of points to the surface measured in grid units, grid size, number of iterations and correct surface topology.

demonstrated in the experiments. Finally, the general variational formulation makes it easy for the reader to include visibility constraints in his/her favorite surface evolution or reconstruction method.

Acknowledgements: The authors thank Dr. Lena Klasén, Director of Sensor Technology at the Swedish Defence Research Agency FOI, for providing the time-of-flight data. Research support from the Swedish Research Council and U.C. MICRO Program is gratefully acknowledged.

References

[1] E.Boyer and J-S. Franco. A hybrid approach for computing visual hulls of complex objects. In *Proc. Conf. Computer Vision and Pattern Recognition*, volume 1, pages 695–701, 2003.

[2] O. Faugeras and R. Keriven. Variational principles, surface evolution, PDEs, level set methods, and the stereo problem. *IEEE Transactions on Image Processing*, 7(3):336–344, 1998.

[3] B. Goldlücke and M. Magnor. Weighted minimal hypersurfaces and their applications in computer vision. In *European Conference on Computer Vision*, volume 2, pages 366–378, Prague, Czech Republic, 2004.

[4] R. I. Hartley. Chirality. *International Journal of Computer Vision*, 26(1):41–61, 1998.

[5] R. I. Hartley and A. Zisserman. *Multiple View Geometry in Computer Vision*. Cambridge University Press, 2000.

[6] H. Jin, S. Soatto, and A.J. Yezzi. Multi-view stereo beyond lambert. In *Proc. Conf. Computer Vision and Pattern Recognition*, Madison, Wisconsin, 2003.

[7] V. Kolmogorov and R. Zabih. Multi-camera scene reconstruction via graph cuts. In *Proc. European Conf. on Computer Vision*, 2002.

[8] K. N. Kutulakos and S. M. Seitz. A theory of shape by space carving. *Proc. Int. Conf. on Computer Vision*, 1999.

[9] M. Lhuillier and L. Quan. Surface reconstruction by integrating 3d and 2d data of multiple views. In *Int. Conf. Computer Vision*, pages 1313–1320, Nice, France, 2003.

[10] W.E. Lorensen and H.E. Cline. Marching cubes: a high resolution 3d surface reconstruction algorithm. *Computer Graphics (Siggraph'87)*, 21(4):163–169, 1987.

[11] A. Manessis, A. Hilton, P. Palmer, P. McLauchlan, and X. Shen. Reconstruction of scene models from sparse 3D structure. In *Proc. Conf. Computer Vision and Pattern Recognition*, volume 2, pages 666–671, 2000.

[12] D. Nister. Calibration with robust use of cheirality by quasi-affine reconstruction of the set of camera projection centres. In *Proc. Int. Conf. on Computer Vision*, volume 2, pages 116–123, 2001.

[13] S. J. Osher and R. P. Fedkiw. *Level Set Methods and Dynamic Implicit Surfaces*. Springer Verlag, 2002.

[14] M. Pollefeys, L. Van Gool, M. Vergauwen, F. Verbiest, K. Cornelis, J. Tops, and R. Koch. Visual modeling with a hand-held camera. *International Journal of Computer Vision*, 59(3):207–232, 2004.

[15] J.B. Rosen. The gradient projection method for nonlinear programming: Part II, nonlinear constraints. *J. Society for Industrial and Applied Mathematics*, 9:514–532, 1961.

[16] G. Sapiro, R. Kimmel, D. Shaked, B.B. Kimia, and A.M. Bruckstein. Implementing continuous-scale morphology via curve-evolution. *Pattern Recognition*, 26(9):1363–1372, 1993.

[17] J.E. Solem and A. Heyden. Reconstructing open surfaces from unorganized data points. In *International Conference on Computer Vision and Pattern Recognition, Washington DC*, 2004.

[18] J.E. Solem and F. Kahl. Surface reconstruction from the projection of points, curves and contours. In *2nd Int. Symposium on 3D Data Processing, Visualization and Transmission, Thessaloniki, Greece*, 2004.

[19] J.E. Solem and N.C. Overgaard. A geometric formulation of gradient descent for variational problems with moving surfaces. In *Scale Space*, 2005.

[20] R. Szeliski. Rapid octree construction from image sequences. *CVGIP: Image Underst.*, 58(1):23–32, 1993.

[21] C. J. Taylor. Surface reconstruction from feature based stereo. In *Int. Conf. Computer Vision*, pages 184–190, Nice, France, 2003.

[22] H.K. Zhao, T. Chan, B. Merriman, and S. Osher. A variational level set approach to multiphase motion. *J. Computational Physics 127*, pages 179–195, 1996.

[23] H.K. Zhao, S. Osher, B. Merriman, and M. Kang. Implicit and non-parametric shape reconstruction from unorganized points using a variational level set method. In *Computer Vision and Image Understanding*, pages 295–319, 2000.